Real-time monitoring of DNA immobilization and detection of DNA polymerase activity by a microfluidic nanoplasmonic platform

Accepted Manuscript

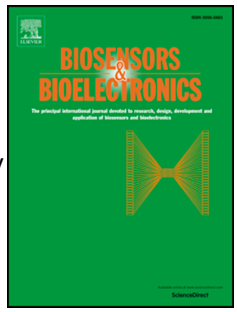

Real-time monitoring of DNA immobilization and detection of DNA polymerase activity by a microfluidic nanoplasmonic platform

Johanna Roether, Kang-Yu Chu, Norbert Willenbacher, Amy Q. Shen, Nikhil Bhalla

PII: S0956-5663(19)30607-4

DOI: https://doi.org/10.1016/j.bios.2019.111528

Article Number: 111528

Reference: BIOS 111528

To appear in: *Biosensors and Bioelectronics*

Received Date: 29 May 2019

Revised Date: 18 July 2019

Accepted Date: 20 July 2019

Please cite this article as: Roether, J., Chu, K.-Y., Willenbacher, N., Shen, A.Q., Bhalla, N., Real-time monitoring of DNA immobilization and detection of DNA polymerase activity by a microfluidic nanoplasmonic platform, *Biosensors and Bioelectronics* (2019), doi: https://doi.org/10.1016/j.bios.2019.111528.

Real-time monitoring of DNA immobilization and detection of DNA polymerase activity by a microfluidic nanoplasmonic platform

Johanna Roether[a,b], Kang-Yu Chu[a], Norbert Willenbacher[b], Amy Q. Shen[a], Nikhil Bhalla[a,c]

[a] *Micro/Bio/Nanofluidics Unit, Okinawa Institute of Science and Technology, Onna, Okinawa 904-0495, Japan.*
[b] *Institute of Mechanical Process Engineering and Mechanics, Applied Mechanics Group, Karlsruhe Institute of Technology, 76137 Karlsruhe, Germany.*
[c] *Nanotechnology and Integrated Bioengineering Centre (NIBEC), School of Engineering, Ulster University, Jordanstown, Shore Road, BT37 0QB, Northern Ireland, United Kingdom*

Abstract

DNA polymerase catalyzes the replication of DNA, one of the key steps in cell division. The control and understanding of this reaction owns great potential for the fundamental study of DNA-enzyme interactions. In this context, we developed a label-free microfluidic biosensor platform based on the principle of localized surface plasmon resonance (LSPR) to detect the DNA-polymerase reaction in real-time. Our microfluidic LSPR chip integrates a polydimethylsiloxane (PDMS) channel bonded with a nanoplasmonic substrate, which consists of densely packed mushroom-like nanostructures with silicon dioxide stems (∼40 nm) and gold caps (∼22 nm), with an average spacing of 19 nm. The LSPR chip was functionalized with single-stranded DNA (ssDNA) template (T30), spaced with hexanedithiol (HDT) in a mo-

Email addresses: amy.shen@oist.jp (Amy Q. Shen), n.bhalla@ulster.ac.uk (Nikhil Bhalla)

lar ratio of 1:1. The DNA primer (P8) was then attached to T30, and the second strand was subsequently elongated by DNA polymerase assembling nucleotides from the surrounding fluid. All reaction steps were detected in-situ inside the microfluidic LSPR chip, at room temperature, in real-time, and label-free. In addition, the sensor response was successfully correlated with the amount of DNA and HDT molecules immobilized on the LSPR sensor surface. Our platform represents a benchmark in developing microfluidic LSPR chips for DNA-enzyme interactions, further driving innovations in biosensing technologies.

Keywords: LSPR, microfluidic biosensor, DNA polymerase, self-assembled-monolayers (SAM)

1. Introduction

DNA polymerization, mediated by the enzyme polymerase, assembles nucleotides along a single stranded DNA, using the latter as a template. This reaction is one of the key steps in the replication of DNA of all types of cells and organisms. Therefore monitoring a DNA polymerase reaction in real-time is important in many applications. For example, it is crucial to monitor all reaction steps such as primer binding, enzyme binding, elongation along the template, and the release of the enzyme (see Fig 1 a-c) for diagnosis and pharmaceutical drug testing. To meet the demand of real-time monitoring, some labeled sensing approaches have been developed to detect DNA polymerase activity, which includes discontinuous radio-labeled (Benkovic and Cameron, 1995), direct and indirect fluorescence (Shapiro et al., 2005; Seville et al., 1996; Griep, 1995; Ronaghi, 2001), and particle labeled (San-

nomiya et al., 2008) assays at bulk and single molecule level. Most of these methods are either time consuming, laborious, cost inefficient or require the usage of toxic chemical reagents (e.g., radioactive tags/labels).

Among label-free methods, quartz crystal microbalance (QCM) serves as a simple and powerful tool for real-time measurements (Matsuno et al., 2001), but the measurement response is sensitive to changes in the bulk solution, therefore the signal leads to an overestimation of the number of bound biomolecules (Bingen et al., 2008). The use of localized surface plasmon resonance (LSPR) techniques has recently emerged as an important label-free sensing technique: it is an optical phenomenon that causes a collective oscillation of valence electrons and subsequent absorption within the ultraviolet-visible (UV-Vis) band of the light spectrum, due to interactions between the incident photons and the conduction band of a noble metal nanostructure (Anker et al., 2010; Hammond et al., 2014; Bhalla et al., 2018a). LSPR is sensitive to the local refractive index around the nanostructures to enable the detection of biomolecule binding events (Mayer and Hafner, 2011). The short decay length of the electromagnetic field in localized surface plasmons makes LSPR relatively insensitive to the bulk effects, thus reducing the sensitivity response to the interference from the bulk solution's refractive index (Szunerits and Boukherroub, 2012).

LSPR biosensors have achieved the detection of bio/chemical processes involving DNA, proteins, biomarkers, enzymes, food-borne pathogens, heavy metals, microbial biofilms and even living eukaryotic cells (Bhalla et al. (2018b)). In reference to DNA based sensing, various LSPR biosensors have been successfully implemented to measure DNA hybridization. In particular,

chip-based (Huang et al., 2012; Soares et al., 2014; Park et al., 2009; Endo et al., 2005) and nanoparticle (Schneider et al., 2013) based approaches have been used for end-point analysis of DNA hybridization, serving as efficient alternatives to conventional polymerase chain reaction (PCR) procedures, enabling highly sensitive quantification of DNA concentrations in solution (Kaye et al., 2017). Kim et al. (Kim et al., 2017) and Baaske et al. (Baaske et al., 2014) recently employed nanorods with whispering gallery modes in microcavities for the detection of DNA/DNA polymerase interactions and conformational changes at a single molecular level. A combined setup of LSPR and electrochemical impedance spectroscopy has also been used for DNA sensing applications (Cheng et al., 2014).

The sensitivity of LSPR based biosensors can be potentially increased by integrating it with microfluidics. This is because the microfluidic systems provide precise control of the fluid flow, reduce sample volume, avoid evaporation and enhance the mixing rate of different reagents which often lead to an increase in the sensitivity of biomolecule detection, when integrated with biosensing technologies (Luka et al., 2015). In addition, reactions involving multiple fluid processing steps can be controlled in an automated manner inside a microfluidic chip, thereby avoiding potential measurement errors resulting from user to user discrepancy. The coupling of microfluidics and biosensors also introduces features such as portability, disposability, and multiplexed analysis of various analytes in a single device. Most importantly, real-time measurements can be realized by taking advantage of the high surface specificity the LSPR technique for sensing applications (Oh et al., 2014; Aćimović et al., 2014). For instance Oh et al. developed an integrated

nanoplasmonic microfluidic chip to detect cell-secreted tumor necrosis factor (TNF)-α cytokines in clinical blood samples (Oh et al., 2014) and to detect cancer markers in serum (Aćimović et al., 2014). Touahir et al. (Touahir et al., 2010) proposed a microfluidic DNA sensing approach based on metal-nanostructure enhanced fluorescence, but this requires fluorescence labeling of the DNA probes. More recently, Haber et al. were able to monitor DNA hybridization in real-time by combining sensor chips with silver nanoprism structures with a microfluidic setup in a label-free manner (Haber et al., 2017). However, to our knowledge, no work on LSPR detection of DNA polymerase reaction in real-time has been reported in literature.

Our work successfully demonstrates, for the first time, a LSPR microfluidic chip to detect the immobilization of single stranded DNA (ssDNA) mixed with spacer molecules (1-Hexadecanethiol, HDT) on gold nanostructures via thiol-chemistry and subsequently detect their interaction with DNA polymerase enzyme in real-time at room temperature. Our LSPR-microfluidic platform is superior in distinguishing each step in the polymerase reaction. For instance, we show that events involving binding of small molecules such as the DNA primer (P8) and nucleotides can easily be detected by our LSPR microfluidic chip in real-time, in contrast to bulk sensors such as QCM. We also show reduced non-specific binding and clear distinction of the polymerase reaction inside the LSPR-microfluidic platform in real-time, when compared to the traditional LSPR measurements without using microfluidics. Our developed LSPR-microfluidic platform may provide a good benchmark sensing platform for DNA-based molecular diagnostics.

2. Materials and Methods

2.1. DNA Immobilization on LSPR substrates

Thiolated DNA-template T30 (S-5'GACGCTAGGATCTGACTGCGCC TCCTCCAT-3 (Hokkaido Gene Design, Japan) was dissolved in TE buffer (100 mM TRIS/10 mM EDTA, pH8), blended in a ratio of 1:1 with the reduction buffer (0.12 M of Di-thiothreitol (DTT): 0.5 M of Phosphate buffered saline (PBS) = 2:1) and henceforth the reduction of T30 took place at room temperature within 6 h. The DNA was then de-salted and the resulting DNA concentration in the TE buffer was measured to be 0.66 μM (nanodrop fluorometer, Thermo Fisher, Japan). The thiolated DNA was then conjugated on the clean gold-based substrates (gold nanostructured LSPR substrates, gold nanostructured LSPR substrate integrated with microfluidics, and substrates for QCM-D) using HDT as a spacer molecule to avoid the steric hindrance, see Figure 1 (step a). The reaction solution containing 0.45 μM DNA and 0.45 μM HDT in TE buffer, was deposited on the substrates or pumped through the microfluidic chips to initiate the immobilization within 16 h, all performed at room temperature. After the immobilization, the functionalized substrates were washed three times for 15 min with 1$\times$ PBS.

2.2. In-vitro DNA polymerase reaction

The functionalized chips were impinged with primer solution, figure 1 step b, (0.1 μM primer P8 (5-ATGGAGGA-3, Invitrogen), 0.5 μM dNTPs (Taraka Bio Inc., Japan), diluted in polymerase reaction buffer (New England Biolabs, NEB), prepared according to manufacturer's manual. The primer binding was carried out for 15 min. After following threefold PBS

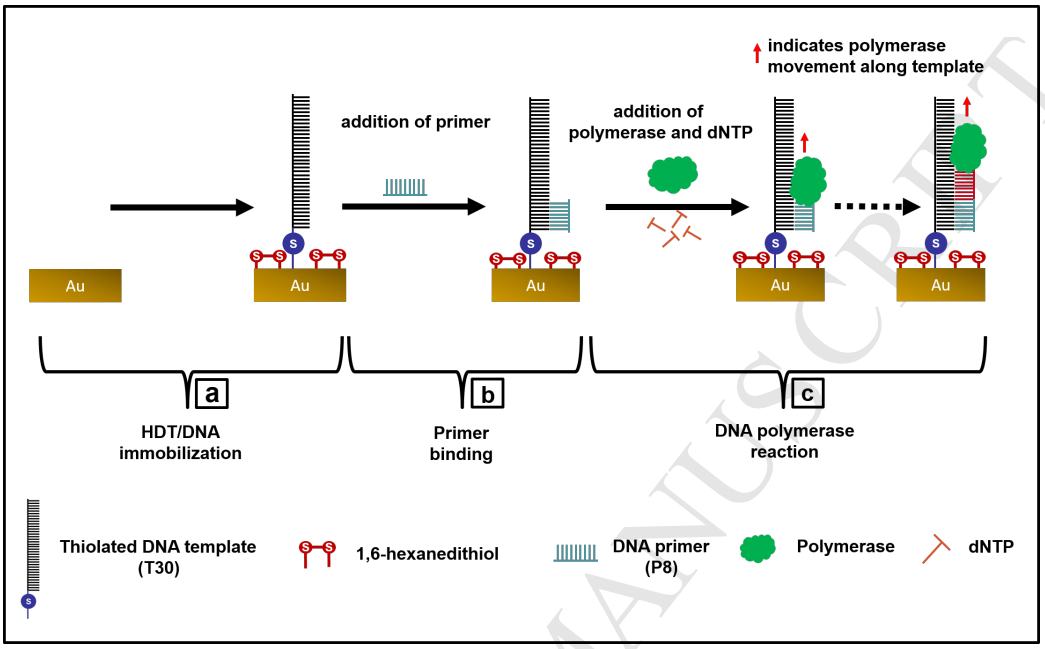

Figure 1: Reaction scheme on a gold (Au) LSPR substrate, involving (a) an immobilized ssDNA template (T30) with HDT; (b) addition of primer sequence P8, and (c) Klenow fragment of DNA-polymerase along with dNTPs. Polymerase catalyzes the formation of the complementary DNA strand by assembling dNTPs from the surrounding media.

wash (15 min), the polymerase reaction mixture (0.0625 U/ml of polymerase enzyme (from E .Coli, Klenow Fragment, purchased from NEB) was added, see Figure 1 (step c). Under the assumption of ideal reaction conditions, the given amount of enzyme should convert all dNTPs contained in the reaction mixture within a few minutes. However, we extended this reaction step for 2.5 h to investigate secondary remodeling processes. Finally, another threefold PBS wash was performed in order to remove non-specifically bound reactants and the remaining enzyme complexes.

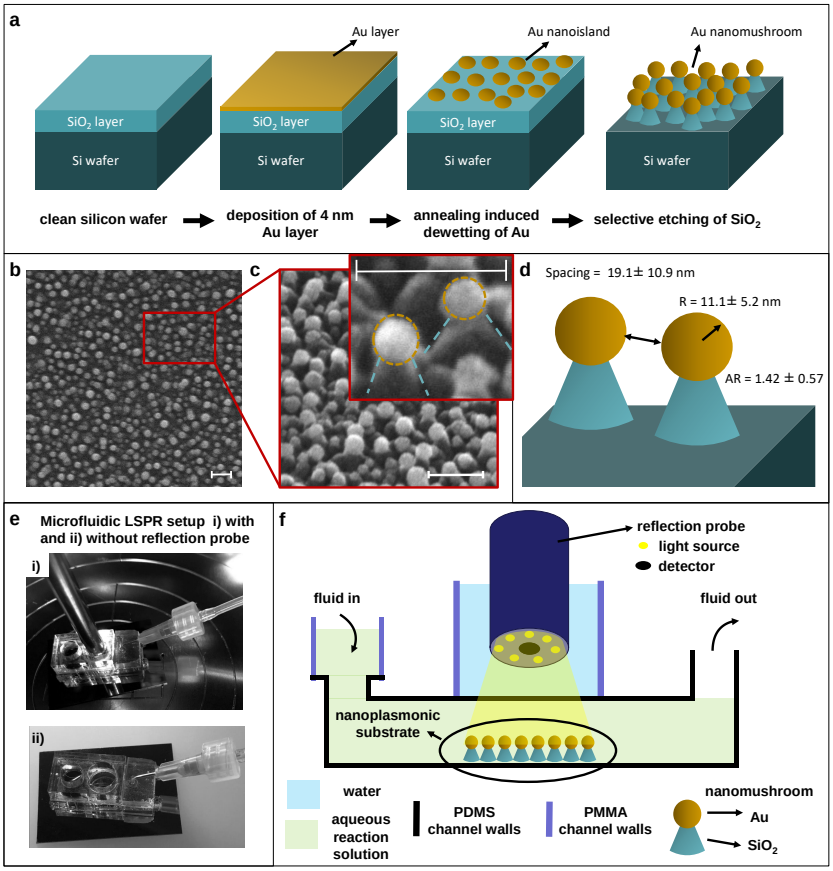

Figure 2: Fabrication of LSPR-microfluidic platform. (a) Manufacturing of plasmonic surfaces starting from a bare silicon wafer on which a 4 nm gold layer is first deposited, thermally de-wetted before the SiO_2 layer is selectively etched using SF_6 plasma. (b) Scanning electron microscopy (SEM) images show the Au nanostructures in horizontal plane, top view, (c) side view with 40° tilted, with the inset showing the zoomed in view of two pillared nanostructures with the gold cap and SiO_2 stem, outlined in yellow and turquoise, respectively. All scale bars represent 100 nm. (d) Schematic of the inset in (c) showing the detailed dimensions of the nanopillar structures.

The mean Au cap radius is $\sim 11.1 \pm 5.2$ nm. (e) Snap shots of a LSPR-microfluidic chip, in operation with indented reflection probe (i) and without (ii). In both cases the fluid inlet reservoir and the outlet tubing are shown. (f) Schematic of the microfluidic nanoplasmonic chip consisting of the bottom nanoplasmonic substrate, a PDMS and a poly(methyl methacrylate) (PMMA) substrate.

2.3. Fabrication of LSPR substrates

The fabrication of LSPR gold nanostructures was based on a well established three step process consisting of gold deposition, de-wetting and glass etching (Bhalla et al., 2018b). Briefly, a 4 nm gold film was evaporated on a silicon wafer coated with 500 nm of SiO_2 (KST, Japan) using an electron beam evaporator (MEB550S2-HV, PLASSYS Bestek, France). The film was then annealed at 560 °C for 3.5 h, forming individual gold islands due to solid state de-wetting of the gold film (see Fig. 2 a-d). These nanoislands were transformed to pillar-like nanostructures with SiO_2 stems and Au caps by selective etching of the SiO_2 layer. Reactive ion SF_6 plasma was applied using an inductively coupled plasma chemical vapor deposition equipment (Plasmalab 100, Oxford Instruments, UK).

2.4. Characterization of LSPR substrates

Scanning electron microscopy (SEM) was used to characterize the size and morphology of the Au nanostructures. The average diameter and cap-to-cap distance were obtained by using the particle analysis module in ImageJ software(Schindelin et al., 2012). The Au caps were assumed to be circular and bright in the image with threshold type processing. The detailed morphology of Au nanostructures were analyzed after applying a contrast threshold with three independent images.

2.5. Fabrication of microfluidic chips with LSPR substrates

The microfluidic LSPR chip involves three-layered substrates: the LSPR Si substrate containing Au plasmonic nanostructures, a transparent Polydimethylsiloxane (PDMS) layer, and a transparent poly(methyl methacry-

late) (PMMA) layer. To ensure tight bonding between the LSPR substrate and PDMS, the Si wafer (2×4 cm) was covered by a mask with open circles of 5 mm in diameter. This ensures that Au nanostructures were fabricated only inside the circular areas during the Au evaporation, annealing and etching steps. The PDMS containing a central circular reaction area of 19.6 mm^2 was then bonded with the LSPR substrate by using oxygen plasma. On top of the PDMS layer, a poly-methyl-methacrylate (PMMA) cuboid (25×15×8 mm) with a cylindrical hole (8 mm in diameter) was attached by using a double sided tape. This PMMA layer served as a water reservoir for indentation of the fibre optics, consisting of the LSPR light source and the detector (see detailed schematic in Fig. 2 e-f). The inlet of the PDMS channel was connected to the tubing system using a connector needle. To introduce new reactants and carry out the necessary washing steps, fluids were withdrawn with a syringe pump at a flow rate of 50 μl/min. This flow rate avoided bubble formation and enabled stable flow in the microfluidic chip.

2.6. LSPR measurements on bare nanoplasmonic substrates

A customized setup consisting of a stage, a spectrometer (USB4000-UV-VIS-ES, Ocean Optics, Japan), a combined light source and detecting probe (Ocean Optics, Japan) and an optical fiber (Ocean Optics, Japan) connecting the latter was assembled to measure light reflected by the nanoplasmonic structures. Prior to each measurement, bright and dark reference spectra were recorded using a custom matlab routine developed in our lab. This allowed the automatic calculation of maximum wavelength and peak shifts from the LSPR in the Au nanostructures. After an initial reflection measurement of the bare LSPR substrate, the whole reaction was performed as

described in sections 2.1 and 2.2. Briefly, 80 μl of template and spacer solution were poured into the PMMA well fixed on the nanostructured LSPR substrate and after 16 h of immobilization, primer binding and polymerase reaction was performed. After the last PBS washing step, the LSPR signal of the functionalized chip was measured. For each of the conditions, at least three LSPR substrates were used for measurements and shifts of the absorption maximum $\Delta\lambda$ were calculated by subtracting the initial maximum wavelength of each individual LSPR substrate λ_{blank}. To avoid salt residues, we decreased the PBS concentration of the washing solution step-wise and finally washed it with de-ionized water. After drying with compressed air, LSPR signals were measured.

For the characterization of the refractive index sensitivity, freshly prepared bare LSPR substrates were used. Water (RI = 1.333), acetone (RI = 1.356), isopropanol (RI = 1.376), mineral oil (RI = 1.466), and toluene (RI = 1.496) were poured into the cylindrical well and the wavelength spectrum of the reflected light was measured while the probe was indented into the solvents. The sensitivity was calculated as the slope of the linear regression of the wavelength maximum λ_{max} plotted over the solvents' refractive index RI. The refractive index reference values were measured at room temperature using a spectrophotometer (UV-Vis 1800, Shimadzu, Japan) and compared to literature values.

2.7. Real-time microfluidic LSPR measurements

In real-time measurements, the developed LSPR microfluidic chip (see Fig. 2 e-f) was used at room temperature. The washing liquids and reaction mixtures were introduced through the inlet reservoir and withdrawn by a

syringe pump. The spectrum was recorded continuously every 15 s during the entire duration of the experiment (∼20 h). The wavelength shifts were captured at the end of each reaction step, presented as the mean value with standard deviation based on at least three independent experiments. The microfluidic setup has a closed fluid loop to prevent solvent evaporation.

3. Results and Discussion

3.1. Characterization of bare LSPR substrates for the detection of DNA polymerase reaction

The sensitivity of the nanoplasmonic substrate was first verified by using different solvents with known refractive indices (RI) in the relevant range for DNA monolayers (i.e., $RI_{ssDNA} \sim 1.45$ and $RI_{dsDNA} \sim 1.52$ (Elhadj et al., 2004)). Fig 3 a shows a linear fit ($R^2 = 0.95$) of wavelength shifts versus RI with a slope of 54 ± 6 nm/RIU. This slope is essentially the RI sensitivity of the nanoplasmonic substrate in the range of refractive indices of ssDNA and dsDNA. In addition, we require a minimum of 0.0625 U/ml of polymerase to see changes in LSPR signal and therefore we consider this value as the limit of detection of our sensor. Resulting LSPR spectra from polymerase reaction are shown in Fig 3 b and mean values of three independent experiments are summarized in Fig 3 c. These values were calculated as shifts between the bare LSPR substrate and the LSPR substrate with double stranded DNA after the whole polymerase reaction was completed.

Based on the information shown in Fig 3 a, the theoretical shift caused by the polymerization of double-stranded DNA, $\Delta(\mathrm{RI}) = 0.06$ corresponds to $\Delta\lambda \sim 3.24$ nm. In our DNA polymerase experiment (see condition (E)

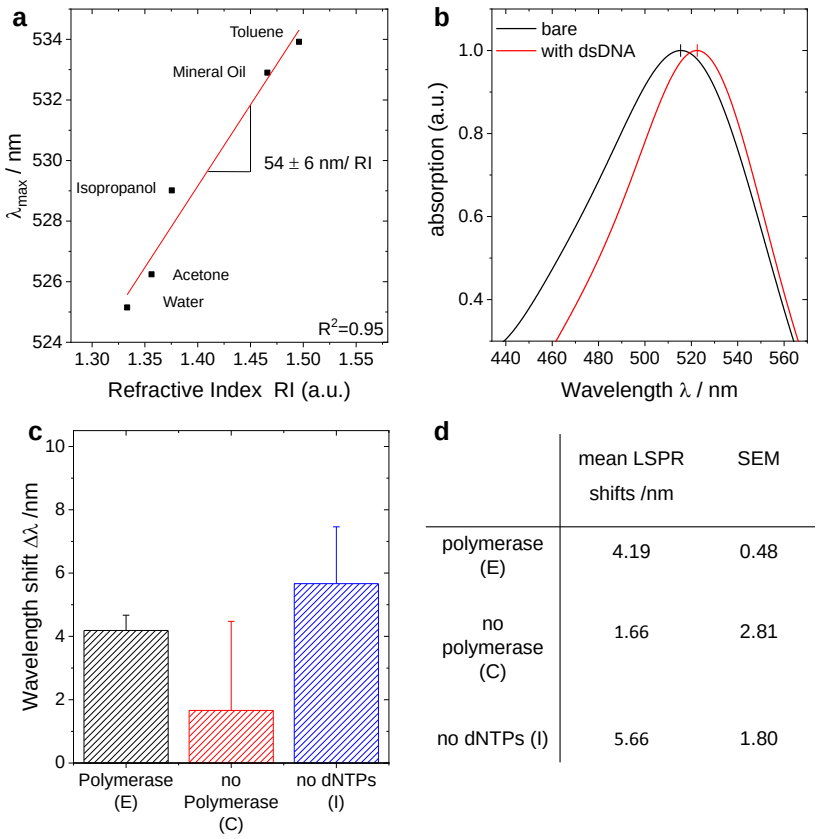

	mean LSPR shifts /nm	SEM
polymerase (E)	4.19	0.48
no polymerase (C)	1.66	2.81
no dNTPs (I)	5.66	1.80

Figure 3: DNA polymerase monitoring using discontinuous LSPR measurements. (a) refractive index sensitivity of the nanoplasmonic substrate in a relevant RI range for DNA layers, calculated by linear regression from LSPR measurements with five different solvents; (b) A typical absorption spectrum of a bare nanoplasmonic substrate and after completing immobilization and elongation of ds30-mers (normalized), showing a wavelength shift $\Delta\lambda$ = 3.8 nm; (c) resulting shifts after completing the whole reaction cycle of the polymerase experiment (E, black), control without enzyme (C, red) and substrate inhibition (I, blue), shown as the mean values of N = 3 experiments. (d) Table summarizing the values in subfigure (c).

in Fig 3 c), a shift of 4.19 ± 0.48 nm was obtained. This shift represents both the immobilization of ssDNA/HDT and the polymerase reaction. In the control experiments without the polymerase enzyme (C, control without enzyme), a mean shift of $\Delta\lambda = 1.66 \pm 2.81$ nm was observed (see Fig 3 c and d). Note that the immobilization of ssDNA/HDT alone causes a shift of 3.50 ± 1.27 nm, which was measured after the immobilization process and the subsequent washing and drying of the LSPR substrate with compressed air. These values were calculated by normalization of wavelength shifts with respect to the blank LSPR substrate prior to the start of the experiment. In contrast, in the control experiment without dNTPs (I, enzyme inhibition), obtained wavelength shifts ($\Delta\lambda = 5.66 \pm 1.80$ nm) were much higher. One potential explanation is that after polymerase molecules attach to the ssDNA, these molecules cannot be released from the DNA strand during the washing steps. This increases the local optical density on the sensor surface, which in turn causes an additional red shift. Most importantly, in order to avoid effects of the liquid meniscus in the light path, the actual wavelength shifts need to be evaluated while immersing the probe (see measurement of RIs of different solvents) or after drying the LSPR surfaces with compressed air. The drying of the substrate can precipitate salts from the buffer solution, which might remain on the nanostructures of the LSPR substrate, leading to larger LSPR shifts. This can affect the refractive index on the LSPR substrate, which may lead to poor reproducibility of the LSPR measurements. An immediate wash with DI water avoids the salt precipitation from buffer solution. However, the DNA/HDT self-assembled monolayer (SAM) optical density and/or functionality might be affected by the inappropriate buffer

condition, which can cause indistinguishable LSPR shifts among experiments and controls. An improvement in the combination of these two processing steps (drying to avoid meniscus and washing with DI water) can enhance the specificity in the LSPR measurements and ensure the bio-functionality for subsequent reaction steps. In the next section we show that the use of microfluidics can eliminate many of the issues raised above by controlling the fluid in an automated manner.

3.2. LSPR microfluidic chip for real-time monitoring of DNA immobilization and polymerase activity

Incorporating nanoplasmonic substrates in a microfluidic system allowed real-time measurements of complete ssDNA/HDT immobilization and polymerization reaction steps. An exemplary sensogram of our LSPR experiment is shown in Fig 4 a where LSPR wavelength shifts relative to the functionalized chip (PBS wash after immobilization) are plotted. Note that the response time of our LSPR sensor is 1 s. However, this sensor response time is tunable with software where the data was acquired every 15 s during the 20 h real-time measurement. The acquisition time then defines the response time to ensure that there is no overload of the data in the hard drive of our in-lab measurement system. Figure 4b compares the total red shifts in the LSPR signal of a bare LSPR/microfluidic chip in PBS and dsDNA after polymerization reaction. It is possible to track the continuous red shifts in the LSPR wavelength maximum during the first 12 h of the ssDNA/HDT immobilization process. After 12 h, the LSPR signal starts to stabilize and saturation was achieved at 16 h, which was considered as the end of the ssDNA/HDT immobilization. In the following primer binding and washing

steps, around $\sim$ 1.49 nm shifts were observed. After addition of polymerase, a shift of $\sim$ 1.1 nm was detected. This was most likely caused by the binding of the enzyme at the DNA strands and by the binding of additional dNTPs to the DNA strand. After the first 15 min of the elongation period, a small wavelength shift ($\sim$ 0.5 nm) was observed. This time scale fits well with the theoretical reaction speed of 0.25 units of enzyme per reaction (0.0625 U/ml) that are estimated to react with all the available dNTPs (10 μmoles) within 16 min. It should be noted that only a small fraction of the available dNTPs can be bound to the immobilized template, thus the elongation reaction completed much sooner than 16 min, which in turn serves as an explanation for the stabilization of the LSPR signal during the remaining elongation time. At the end of the reaction and the final washing step, the release of the heavy enzyme molecules caused a blue shift of 1.2 nm. In the control experiment (C) without polymerase enzyme, varied amounts of LSPR shifts occurred after the reaction was accomplished. This is attributed to various amounts of non-specifically attached dNTPs in between adjacent DNA molecules. The non-specific attachment creates a large standard deviation in this control experiment (see figure 4c), resulting in low significance of this data as compared to the polymerase reaction (p=0.1744, unpaired one-tailed t-test). However, this non-specific attachment of dNTPs could be reduced by changing the spacing between ssDNA molecules by varying the ratio of DNA/HDT in the first step of the experiment. Despite different amounts of non-specific attachment of dNTPs, the polymerase reaction (E, black curve in fig 4a) and the control without enzyme (C, red curve in fig 4a) can easily be distinguished in real-time. Moreover, in both control and experimental

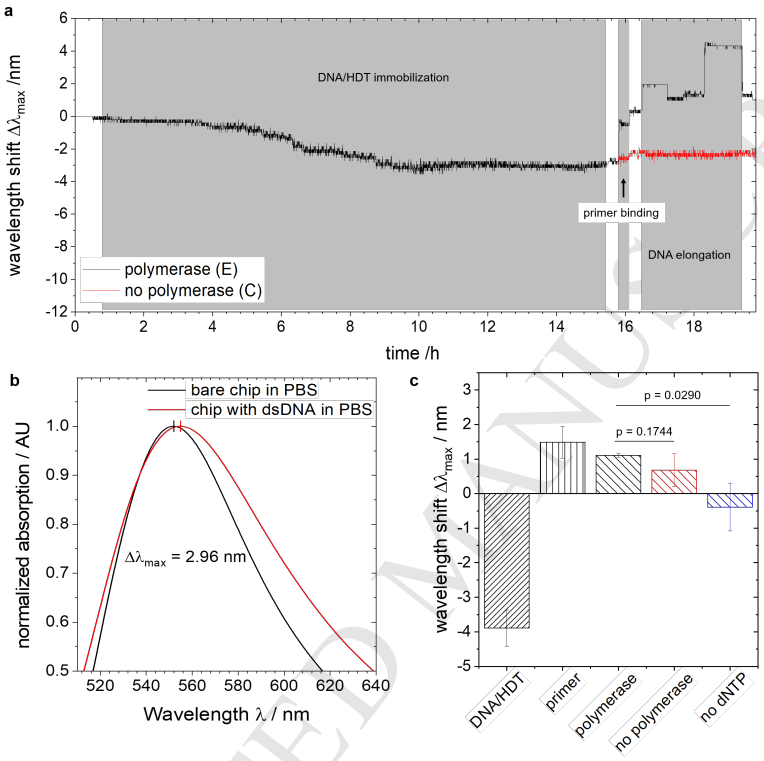

Figure 4: Label-free real-time DNA/HDT immobilization and polymerase activity monitoring using LSPR measurements. (a) Real-time sensogram showing the shift in the maximum wavelength of the reflected light during immobilization of DNA and HDT, primer binding, DNA elongation and intermediate washing steps. (b) A sample reflection spectra of bare microfluidic chip and the chip with ds30-mer showing a total wavelength shift of 2.7 nm, (c) and mean wavelength shifts from each step, calculated from 6 polymerase reactions and 3 controls (no polymerase and no dNTPs) experiments, respectively. Error bars represent standard error of mean. The polymerase versus "no dNTP" is significant with $p < 0.05$.

conditions, no significant wavelength shifts were detected due to the change of buffer solutions, indicating that the buffer effects can be neglected in these LSPR experiments (Diéguez et al., 2009). This is crucial for comparison of individual steps in a continuous reaction inside the microfluidic chip (where fluid control is automated) which often requires different buffer solutions for biochemical reasons. A total shift of $\Delta\lambda_{\max} = 2.96$ nm in the LSPR maximum wavelength was observed after polymerization reaction was completed (see Fig 4 b). An experimental cycle consists of the relative shifts during ssDNA/HDT immobilization (mean of -3.89 ± 0.64 nm), primer binding (mean of 1.49 ± 0.46 nm) and elongation (mean of 1.11 ± 0.06 nm). Normalize by the wavelength from the functionalized chip in PBS (step 3), the mean values of all the shifts are summarized in Fig 4 c. The most obvious shifts were obtained during ssDNA/HDT immobilization and elongation steps, whereas during primer binding only one significant shift occurred.

In contrast, the positive control condition with no dNTPs, leads to a slight blue shift of -0.39 ± 0.98 nm. This is due to the specific binding of polymerase which is expected as no elongation takes place and the polymerase enzyme has no chance to be released from the ssDNA. However, standard one-tailed, t-test reveals that this experiment is significant when compared to the polymerase reaction as the value p=0.0290. This also shows that with the use of microfluidics, certain amount of non-specific attachment due to inefficient washing in discontinuous LSPR measurements (as seen from figure 3) can be minimized.

To validate the results from the microfluidic LSPR sensing system we also used QCM-D to monitor all the steps involved in the polymerase re-

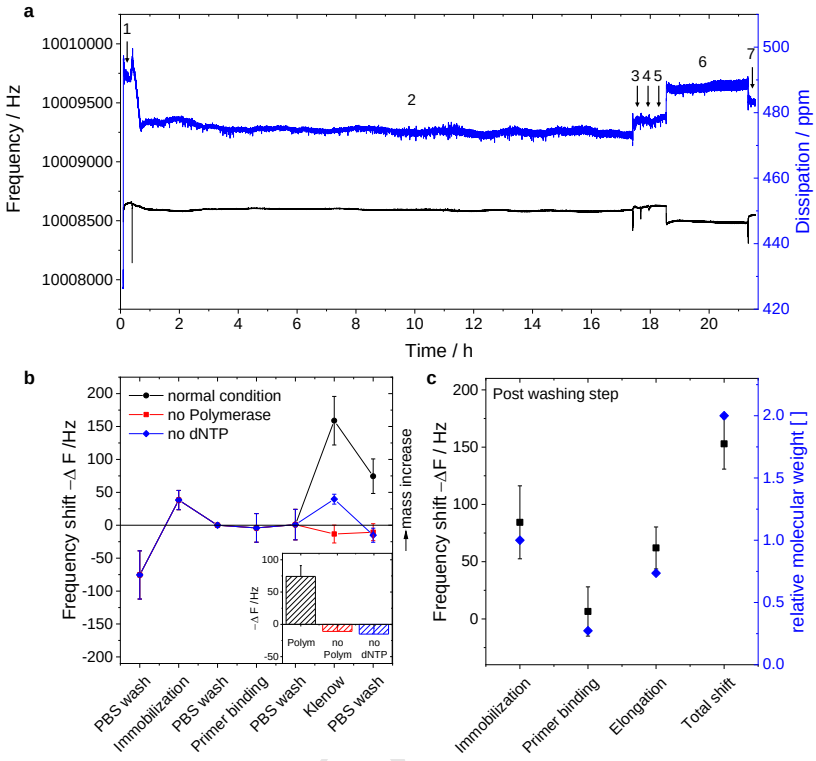

Figure 5: DNA polymerase monitoring with QCM-D. (a) Real sensogram showing the temporal course of frequency (black) and dissipation (blue) during immobilization of DNA (2); primer binding (4), DNA elongation (6) and all corresponding washing steps (1,3,5,7). (b) Frequency shifts during the aforementioned reaction steps of the polymerase reaction (E, black circles), control without enzyme (C, red squares) and substrate inhibition (I, blue diamonds), results from N $\geq$ 3 independent experiments, shown as mean and standard deviation. In the inset, the frequency shift during the crucial elongation step is highlighted. It was calculated as shift from washing before elongation to washing after elongation. (c) Proof of quantitativeness of QCM-D sensing by correlating the step-wise shifts, acquired at the end of each washing step (in PBS buffer) with the molecular weight that is theoretically bound during the corresponding step. Values are normalized to the molecular weight of T30 (~9190 g/mol). More details can be found in part 1 of the supplementary information file.

action. Figure 5a shows both the frequency (black curve) and dissipation (blue curve) changes in real-time caused by immobilization of ssDNA and subsequent elongation of dsDNA strands upon completion of the aforementioned reaction steps. Fig. 5b displays the shifts in the frequency for each step involved in the reaction and Fig. 5c shows the quantitative analysis of QCM-D where frequency shifts are correlated with the molecular weight of the mass bound on the surface of the QCM-D. Fig. 5b illustrates that the shifts upon primer binding cannot be distinguished from PBS wash as minute mass changes upon binding of primer is masked by the bulk effects from the buffer. Nevertheless, the QCM-D results suggest that the wavelength shifts in the LSPR are true signatures of the polymerase activity. More details on the QCM-D measurement principles and discussion on Figure 5 can be found in the supplementary information.

4. Conclusion

We demonstrated the use of nanoplasmonic LSPR technology coupled with microfluidics to monitor the formation of SAMs of ssDNA, and subsequently detect the interaction of DNA with the DNA polymerase enzyme, in real-time and label-free manner. The nanoplasmonic structures, fabricated by thermal de-wetting and reactive ion etching of Au, possessed a RI sensitivity of 54 ± 6 nm/RIU in the relevant range of refractive indices of single and double stranded DNA. The LSPR results for monitoring ssDNA/HDT immobilization and the polymerase reaction were validated by using QCM-D in real-time. Both sensing methodologies, LSPR and QCM-D, suggested that surface functionalization of ssDNA T30 took approximately 12 h, which

is in good accordance with the typical protocols proposing a reaction time of 12 to 16 h. Our work showed that the self-assembly of biochemical monolayers, characterization of enzyme kinetics and inhibition reactions under physiological conditions could now be tested by using labe–free LSPR in real-time with limited human intervention during the course of the reaction. These features are of great interest for the development of nanobiosensors for biomedical applications. Some limitations of our current platform include the lack of temperature control in the microfluidic chip and the need to optimize the HDT/ssDNA surface chemistry to reduce the non-sepcific attachment of dNTP without polymerase enzyme. However, the architecture of the microfluidic chip and the LSPR measurement in the reflection mode allow easy integration of temperature controller in the future. As the polymerase reaction serves as the backbone of DNA sequencing, our LSPR- microfluidic chip can also benefit from the integration of a portable LSPR readout for point of care sequencing applications in the future. Therefore our LSPR microfluidic platform serves as a benchmark system for emerging fields in clinical, pharmaceutical and scientific research which require efficient, easy-to-use, precise methods for comprehensive data collection.

5. Acknowledgements

Authors would like to thank Mr. Hung-Ju Chiang from Okinawa Institute of Science and Technology Graduate University (OIST) for providing help in DNA sample preparations. All authors would also like to acknowledge the support of OIST with subsidy funding from the Cabinet Office, Government of Japan. AQS also acknowledges financial support from the Japanese Society

for the Promotion of Science under grants 17K06173 and 18H01135. KYC and NB also acknowledge the support by the OIST Technology Development and Innovation Center's Proof-of-Concept Program.

6. References

Aćimović, S. S., Ortega, M. A., Sanz, V., Berthelot, J., Garcia-Cordero, J. L., Renger, J., Maerkl, S. J., Kreuzer, M. P., Quidant, R., 2014. Lspr chip for parallel, rapid, and sensitive detection of cancer markers in serum. Nano letters 14 (5), 2636–2641.

Anker, J. N., Hall, W. P., Lyandres, O., Shah, N. C., Zhao, J., Van Duyne, R. P., 2010. Biosensing with plasmonic nanosensors. In: Nanoscience And Technology: A Collection of Reviews from Nature Journals. World Scientific, pp. 308–319.

Baaske, M. D., Foreman, M. R., Vollmer, F., 2014. Single-molecule nucleic acid interactions monitored on a label-free microcavity biosensor platform. Nature nanotechnology 9 (11), 933–939.

Benkovic, S. J., Cameron, C. E., 1995. [20] kinetic analysis of nucleotide incorporation and misincorporation by klenow fragment of escherichia coli dna polymerase i. In: Campbell, J. L. (Ed.), DNA replication. Vol. 262 of Methods in enzymology, 0076-6879. Academic, San Diego, Calif. and London, pp. 257–269.

Bhalla, N., Chiang, H.-J., Shen, A. Q., 2018a. Cell biology at the interface of nanobiosensors and microfluidics. Methods in cell biology 148, 203–227.

Bhalla, N., Sathish, S., Sinha, A., Shen, A. Q., 2018b. Large-scale nanophotonic structures for long-term monitoring of cell proliferation. Advanced Biosystems 2 (4), 1700258.

Bingen, P., Wang, G., Steinmetz, N. F., Rodahl, M., Richter, R. P., 2008. Solvation effects in the quartz crystal microbalance with dissipation monitoring response to biomolecular adsorption. a phenomenological approach. Analytical chemistry 80 (23), 8880–8890.

Cheng, X. R., Hau, B. Y. H., Endo, T., Kerman, K., 2014. Au nanoparticle-modified dna sensor based on simultaneous electrochemical impedance spectroscopy and localized surface plasmon resonance. Biosensors & bioelectronics 53, 513–518.

Diéguez, L., Darwish, N., Mir, M., Martínez, E., Moreno, M., Samitier, J., 2009. Effect of the refractive index of buffer solutions in evanescent optical biosensors. Sensor Letters 7 (5), 851–855.

Elhadj, S., Singh, G., Saraf, R. F., 2004. Optical properties of an immobilized dna monolayer from 255 to 700 nm. Langmuir 20 (13), 5539–5543.

Endo, T., Kerman, K., Nagatani, N., Takamura, Y., Tamiya, E., 2005. Label-free detection of peptide nucleic acid-dna hybridization using localized surface plasmon resonance based optical biosensor. Analytical chemistry 77 (21), 6976–6984.

Griep, M. A., 1995. Fluorescence recovery assay: a continuous assay for processive dna polymerases applied specifically to dna polymerase iii holoenzyme. Analytical biochemistry 232 (2), 180–189.

411 Haber, J. M., Gascoyne, P. R. C., Sokolov, K., 2017. Rapid real-time recir-
412 culating pcr using localized surface plasmon resonance (lspr) and piezo-
413 electric pumping. Lab on a chip 17 (16), 2821–2830.

414 Hammond, J. L., Bhalla, N., Rafiee, S. D., Estrela, P., 2014. Localized sur-
415 face plasmon resonance as a biosensing platform for developing countries.
416 Biosensors 4 (2), 172–188.

417 Huang, C., Ye, J., Wang, S., Stakenborg, T., Lagae, L., 2012. Gold nanor-
418 ing as a sensitive plasmonic biosensor for on-chip dna detection. Applied
419 Physics Letters 100 (17), 173114.

420 Kaye, S., Zeng, Z., Sanders, M., Chittur, K., Koelle, P. M., Lindquist, R.,
421 Manne, U., Lin, Y., Wei, J., 2017. Label-free detection of dna hybridization
422 with a compact lspr-based fiber-optic sensor. The Analyst 142 (11), 1974–
423 1981.

424 Kim, E., Baaske, M. D., Schuldes, I., Wilsch, P. S., Vollmer, F., 2017. Label-
425 free optical detection of single enzyme-reactant reactions and associated
426 conformational changes. Science advances 3 (3), e1603044.

427 Luka, G., Ahmadi, A., Najjaran, H., Alocilja, E., DeRosa, M., Wolthers,
428 K., Malki, A., Aziz, H., Althani, A., Hoorfar, M., 2015. Microfluidics inte-
429 grated biosensors: A leading technology towards lab-on-a-chip and sensing
430 applications. Sensors (Basel, Switzerland) 15 (12), 30011–30031.

431 Matsuno, H., Niikura, K., Okahata, Y., 2001. Direct monitoring kinetic stud-
432 ies of dna polymerase reactions on a dna-immobilized quartz-crystal mi-
433 crobalance. Chemistry - A European Journal 7 (15), 3305–3312.

Mayer, K. M., Hafner, J. H., 2011. Localized surface plasmon resonance sensors. Chemical reviews 111 (6), 3828–3857.

Oh, B.-R., Huang, N.-T., Chen, W., Seo, J. H., Chen, P., Cornell, T. T., Shanley, T. P., Fu, J., Kurabayashi, K., 2014. Integrated nanoplasmonic sensing for cellular functional immunoanalysis using human blood. ACS nano 8 (3), 2667–2676.

Park, K. H., Kim, S., Yang, S.-M., Park, H. G., 2009. Detection of dna immobilization and hybridization on gold/silver nanostructures using localized surface plasmon resonance. Journal of Nanoscience and Nanotechnology 9 (2), 1374–1378.

Ronaghi, M., 2001. Pyrosequencing sheds light on dna sequencing. Genome Research 11 (1), 3–11.

Sannomiya, T., Hafner, C., Voros, J., 2008. In situ sensing of single binding events by localized surface plasmon resonance. Nano letters 8 (10), 3450–3455.

Schindelin, J., Arganda-Carreras, I., Frise, E., Kaynig, V., Longair, M., Pietzsch, T., Preibisch, S., Rueden, C., Saalfeld, S., Schmid, B., Tinevez, J.-Y., White, D. J., Hartenstein, V., Eliceiri, K., Tomancak, P., Cardona, A., 2012. Fiji: an open-source platform for biological-image analysis. Nature methods 9 (7), 676–682.

Schneider, T., Jahr, N., Jatschka, J., Csaki, A., Stranik, O., Fritzsche, W., 2013. Localized surface plasmon resonance (lspr) study of dna hybridiza-

tion at single nanoparticle transducers. Journal of Nanoparticle Research 15 (4), 442.

Seville, M., West, A. B., Cull, M. G., McHenry, C. S., 1996. Fluorometric assay for dna polymerases and reverse transcriptase. BioTechniques 21 (4), 664, 666, 668, 670, 672.

Shapiro, A., Rivin, O., Gao, N., Hajec, L., 2005. A homogeneous, high-throughput fluorescence resonance energy transfer-based dna polymerase assay. Analytical biochemistry 347 (2), 254–261.

Soares, L., Csáki, A., Jatschka, J., Fritzsche, W., Flores, O., Franco, R., Pereira, E., 2014. Localized surface plasmon resonance (lspr) biosensing using gold nanotriangles: detection of dna hybridization events at room temperature. The Analyst 139 (19), 4964–4973.

Szunerits, S., Boukherroub, R., 2012. Sensing using localised surface plasmon resonance sensors. Chemical Communications 48 (72), 8999–9010.

Touahir, L., Galopin, E., Boukherroub, R., Gouget-Laemmel, A. C., Chazalviel, J.-N., Ozanam, F., Szunerits, S., 2010. Localized surface plasmon-enhanced fluorescence spectroscopy for highly-sensitive real-time detection of dna hybridization. Biosensors & bioelectronics 25 (12), 2579–2585.

Highlights

- Microfluidic biochip with mushroom-like nanoplasmonic structures
- Real-time monitoring of DNA based self-assembled monolayers (SAM)
- On-chip detection of DNA-enzyme interactions by LSPR sensing technique

Declaration of interests

☒ The authors declare that they have no known competing financial interests or personal relationships that could have appeared to influence the work reported in this paper.

☒The authors declare the following financial interests/personal relationships which may be considered as potential competing interests:

On the behalf of all authors, this declaration is signed by the corresponding author: **Nikhil Bhalla**

NIKHIL BHALLA